

# Multi Scale Joint Segmentation and Registration of Image Morphology

Marc Droske, Martin Rumpf

**Abstract**— Multimodal image registration significantly benefits from previous denoising and structure segmentation and vice versa. In particular combined information of different image modalities makes segmentation significantly more robust. Indeed, fundamental tasks in image processing are highly interdependent. A variational approach is presented, which combines the detection of corresponding edges, an edge preserving denoising and the morphological registration via a non-rigid deformation for a pair of images with structural correspondence. The morphology of an image function is split into a singular part consisting of the edge set and a regular part represented by the field of normals on the ensemble of level sets. A Mumford-Shah type free discontinuity problem is applied to treat the singular morphology and the matching of corresponding edges under the deformation. The matching of the regular morphology is quantified by a second contribution which compares deformed normals and normals at deformed positions. Finally, a nonlinear elastic energy controls the deformation itself and ensures smoothness and injectivity. A multi scale approach that is based on a phase field approximation leads to an effective and efficient algorithm. Numerical experiments underline the robustness of the presented approach and show applications on medical images.

**Keywords:** image morphology, non-rigid multimodal registration, nonlinear elasticity, Mumford-Shah approach, multiscale phase field approximation, finite element discretization.

## I. INTRODUCTION

Denoising, segmentation and registration are well established as fundamental tools in image processing. For instance, the revolutionary advances in the development of imaging modalities has enabled clinical researchers to perform precise studies of the immense *variability* of human anatomy. As described in the excellent review by Miller, Trouvé and Younes [1] and the overview article of Grenander and Miller [2], this field aims at automatic detection of anatomical structures and their evaluation and comparison. Different images show corresponding structures at usually nonlinearly transformed positions [3], [4]. As the image modality differs there is usually no correlation of image intensities at corresponding positions. What still remains, at least partially, is the local geometric image structure or “morphology” of corresponding objects. Viola, Wells et al. [5], [6] and Collignon [7] presented an information theoretic approach for the registration of multi-modal images. Their statistical method is based on a maximization of mutual information of images of different modality. Recently, Mellor and Brady [8] presented a multi modal matching algorithm based on a statistical search for relationships between feature

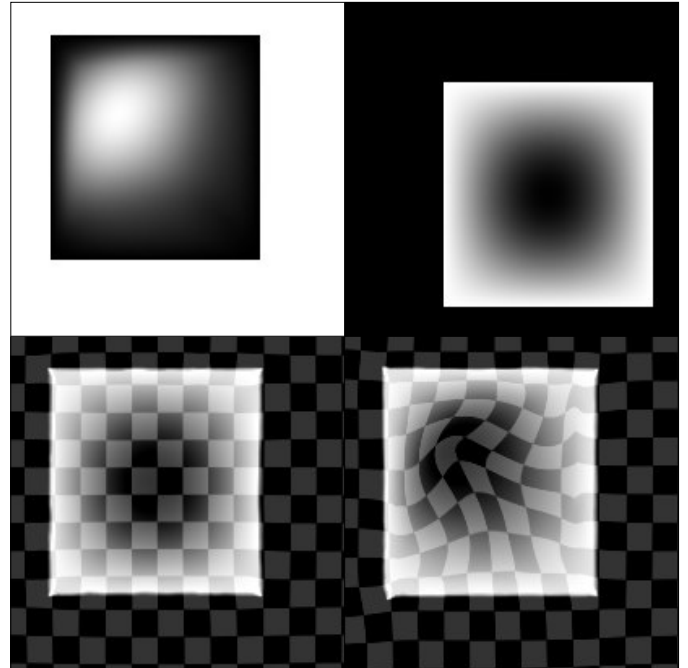


Fig. 1

MORPHOLOGICAL REGISTRATION OF TWO TEST IMAGES. THE TEMPLATE IMAGE IS GENERATED VIA TRANSLATION, NONLINEAR DEFORMATION AND CONTRAST CHANGE OF A REFERENCE IMAGE. THE TOP ROW SHOWS REFERENCE IMAGE  $u_R^0$  AND TEMPLATE IMAGE  $u_T^0$ . ON THE BOTTOM LEFT THE MATCHING RESULT SOLELY BASED ON THE ALIGNMENT OF DEFORMED REFERENCE EDGES AND TEMPLATE EDGES IS DEPICTED. AN OVERLAID PATTERN RENDERS THE DEFORMATION OF A CHECKER BOARD ON THE TEMPLATE DOMAIN. ON THE BOTTOM RIGHT PURE EDGE MATCHING IS COMBINED WITH THE REGISTRATION OF THE REGULAR MORPHOLOGY AND ITS ALIGNMENT OF NORMAL FIELDS.

appearances. In [9] a variational approach not relying on statistics is proposed for morphological image registration. Both approaches do not make explicit use of the segmentation of edges.

Traditionally, the different tools in image processing have been tackled independently. But in fact, robustness and effectiveness of methods can be enhanced significantly by a coupling of these methods. In this paper we will couple edge segmentation and denoising with morphological registration (cf. Fig. 1). Already stated by D’Arcy Thompson in 1917 (cf. [1]), “in a very large part of morphology, our essential task lies in the comparison of related forms rather than the precise definition of each; and the deformation of a complicated figure may be

a phenomenon easy of comprehension, though the figure itself may have left to be unanalyzed and undefined.”

In the last decade, different approaches to couple segmentation with registration have been proposed. Young and Levy [10] used segmentation results for one image to guide the search for edges in consecutive images to resolve boundaries even though they are not well defined in all images. Instead of contour surfaces, Thirion and Gourdan [11] extracted crest lines based on differential characteristics and used them for surface matching. Yezzi, Zöllei and Kapur [12] have simultaneously segmented contours in different images based on an affine matching deformation and an active contour model for the segmentation of implicit curves and surfaces in images similar to the one proposed by Vese and Chan [13]. A related algorithm is described by Unal et al. [14]. They take into account a joint energy for contour curves in different images and relax the curve geometry via a gradient flow. Pre-segmented contours were applied to register functional MR images in an image sequences by Chen et al. [15]. Wyatt and Noble [16] considered Markov random fields in a maximum a posteriori model of joint segmentation and registration. Recently, Feron and Mohammad-Djafari [17] proposed a Bayesian approach for the joint segmentation and fusion of images via a coupling of suitable hidden Markov Models for multi modal images. Applications of joint segmentation and registration were considered by Dohi and Kikinis already in 2001 [18].

In this paper we aim for a variational approach which connects the classification of different portions of image morphology and their proper matching. Two images are called morphologically equivalent, if they only differ by a change of contrast. What structurally remains if we introduce this invariance is the geometry of all level sets of an image. A strict notion of morphology was originally introduced by Matheron [19] and considered further by Caselles, Coll and Morel [20]. They studied the so called upper topographic map (see below). For the morphological registration to be presented here, a proper decomposition of image morphology which distinguishes regular contour surfaces and edge sets is crucial. Furthermore, robustness can be improved by an appropriate edge sensitive image regularization. Thus, we base our approach on the nowadays classical Mumford-Shah approach for image denoising and segmentation in the sense of edge identification. In their pioneering paper, Mumford and Shah [21] proposed the minimization of the following energy functional:

$$E_{MS}[u, S_u] = \int_{\Omega} (u - u_0)^2 d\mathcal{L} + \frac{\mu}{2} \int_{\Omega \setminus S_u} \|\nabla u\|^2 d\mathcal{L} + \eta \mathcal{H}^{d-1}(S_u), \quad (1)$$

where  $u_0$  is the initial image defined on an image domain  $\Omega \subset \mathbb{R}^d$  and  $\mu, \eta$  are positive weights. Here, one asks for a piecewise smooth representation  $u$  of  $u_0$  and a singularity set  $S_u$  consisting of the image edges, such that  $u$  approximates  $u_0$  in a least-squares sense. The intensity function  $u$  ought to be smooth apart from the free discontinuity  $S_u$  and in addition  $S_u$  should be small with respect to the  $d-1$ -dimensional

Hausdorff-measure [22]. Here, we will make use of this approach to regularize images in a suitable way prior to the matching and simultaneously to split image morphology into a regular part related to contour sets of the piecewise smooth portions of an image and a singular part consisting of the edge set. Even though the Mumford-Shah approach itself is not morphological (e.g. intensity scaling may lead to an identification of previously overlooked edges) prominent edges are expected to be uniformly identified basically independent of the image contrast. Mathematically, this Mumford-Shah problem has been treated in the space of functions of bounded variations  $BV$ , more precisely in the specific subset  $SBV$  [22], [23]. A related, alternative decomposition has been proposed by Rudin, Osher and Fatemi [24]. They suggested to minimize  $\|u\|_{BV} + \lambda \|u - u_0\|_{L^2}^2$ .

The free discontinuity set  $S_u$  which represents edges is a morphological quantity. From the regular part of the image, we can extract a second morphological entity representing the ensemble of all level sets. This decomposition of the morphology can be seen as a refinement of the above definition. It will enable us to treat the matching problem for both parts separately incorporating our approach for the registration of normal fields [9]. In particular, the combination prevents us from neglecting strong edges and their proper correlation. In this paper, we will pick up a phase field approximation for the Mumford-Shah functional (1), originally proposed by Ambrosio and Tortorelli [25]. They describe the edge set  $S_u$  by a phase field function  $v$ , which is supposed to be small on  $S_u$  and close to 1 elsewhere. Phase field models are widespread in physics, where they represent a material order parameter and thus describe interfaces in solids or fluids. One asks for minimizers of the energy functional

$$E_{AT}^{\epsilon}[u, v] = \int_{\Omega} \left( (u - u_0)^2 + \frac{\mu}{2} (v^2 + k_{\epsilon}) \|\nabla u\|^2 + \eta \epsilon \|\nabla v\|^2 + \frac{\eta}{4\epsilon} (1 - v)^2 \right) d\mathcal{L}, \quad (2)$$

where  $\epsilon$  is a scaling parameter and  $k_{\epsilon} = o(\epsilon)$  a small positive regularizing parameter. For larger  $\epsilon$  one obtains coarse, blurred representations of the edge sets and corresponding smoother images  $u$ . For decreasing  $\epsilon$  the representation of the edges is successively refined and more and more image details are included. We will make use of this inherent multi scale in a cascadic minimization algorithm. On each scale the regular image morphology is computed on the current image representation. These representations result from the corresponding Ambrosio-Tortorelli approximation.

Eventually, a variational formulation for image registration on a space of general non-rigid deformations leads to an ill-posed problem [26], [27]. This is generally addressed by choosing a suitable regularization. Regularized metrics on infinitesimal deformations of images can be used to define geodesics between images as proposed by Trouvé [28] or more recently by Beg et al. [29]. Alternatively, one can model registration itself as a physically motivated diffusion process as proposed by Thirion [28]. Finally, picking by models from continuum mechanics, one may ask for a deformation that is additionally

controlled by *elastic stresses*. For example see the early work of Bajcsy and Broit [30] and significant extensions in more recent literature [31], [32], [33], [34]. In particular, if large displacements are necessary to ensure a proper match, a regularization based on non-linear elasticity with its built-in control of length, area and volume changes is indispensable. Cohen [35] considered polyconvex elastic functionals and Droske and Rumpf [9] as well as Litke et al. [36] used this type of regularization to guarantee global injectivity and well-posedness. Here, we will incorporate these ideas to avoid local folding in our deformation.

The paper is organized as follows. In Section 2 we present a generalized notion of morphology, which will be used in Section 3 to present a novel variational approach for image registration, that is based on a phase-field technique and takes into account edges as well as classical morphology. In Section 4 we describe the multiscale approach, which is induced by the phase-field approach and is crucial for the energy minimization. Section 5 gives comprehensive details for the required building-blocks for the numerical treatment of the energy relaxation. Section 6 discusses our numerical experiments and results, and Section 7 concludes the paper with final remarks.

## II. REGULAR AND SINGULAR IMAGE MORPHOLOGY

Let us consider different notions of image morphology and develop here a new one that is appropriate for our morphological matching purposes. In mathematical terms, two images  $u, v : \Omega \rightarrow \mathbb{R}$  with  $\Omega \subset \mathbb{R}^d$  for  $d = 2, 3$  are called morphologically equivalent, if they only differ by a change of contrast, i. e., if  $u(x) = (\beta \circ v)(x)$  for all  $x \in \Omega$  and for some function  $\beta : \mathbb{R} \rightarrow \mathbb{R}$  [37], [38]. Here, one usually restricts to contrast changes  $\beta : \mathbb{R} \rightarrow \mathbb{R}$ , which are strictly monotone and continuous functions. Obviously, such a contrast modulation does not change the order and the shape of level sets. Due to the enforced monotonicity, the same holds for the super level sets  $l_c^+[u] = \{x : u(x) \geq c\}$ . Thus, a usual description of the morphology  $\mathcal{M}[u]$  of an image  $u$  is given by the upper topographic map, defined as the set of all these sets

$$\mathcal{M}[u] := \{l_c^+[u] : c \in \mathbb{R}\}.$$

Unfortunately, this set based definition is not feasible for a variational approach we intend to develop here. Furthermore, the restriction to monotone contrast changes conflicts with medical applications and medical morphology. In what follows, we derive an alternative notion based on a regular and a singular morphology. It will directly lead to a variational approach for image matching and allows to get rid of the monotonicity assumption. Let us suppose the image function  $u : \Omega \rightarrow \mathbb{R}$  on an image domain  $\Omega \subset \mathbb{R}^n$  to be in SBV [22]. Hence, we consider functions  $u \in L^1(\Omega)$  of which the derivative  $Du$  is a vector-valued Radon measure with vanishing Cantor part [23]. In fact at edges we allow for jumps and thus infinitely steep gradients concentrated on a sufficiently regular, lower dimensional set, but not for jumps on sets of fractal dimensions. We consider the usual splitting  $Du = D^{ac}u + D^s u$  [22], where  $D^{ac}u$  is the regular part, which is the usual image gradient apart from edges and absolutely continuous with respect to the Lebesgue

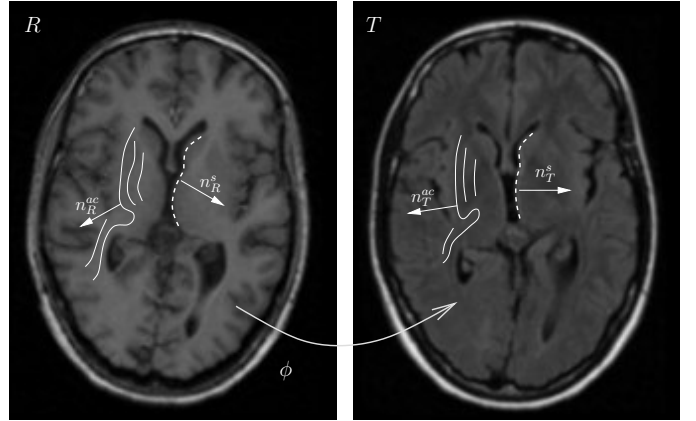


Fig. 2

THE CONCEPT BEHIND MORPHOLOGICAL REGISTRATION: LEVEL SETS OF THE REGULAR MORPHOLOGY OF  $u_R$  CHARACTERIZED BY  $n_R^{ac}$  (WHITE) ARE MAPPED ONTO THE DOMAIN OF  $u_T$  AND COMPARED TO THE REGULAR MORPHOLOGY VIA THE NORMALS  $n_T^{ac}$ . ON THE OTHER HAND MORPHOLOGICAL MATCHING AIMS AT ALIGNING EDGES OF THE SINGULAR MORPHOLOGIES (DASHED) CHARACTERIZED BY  $n_R^s$  AND  $n_T^s$  RESPECTIVELY. THE ALIGNMENT IS ILLUSTRATED BY A NON-RIGID ELASTIC DEFORMATION  $\phi$ .

measure  $\mathcal{L}$  on  $\Omega \subset \mathbb{R}^d$ , and a singular part  $D^s u$ , which represents the jump and is defined on the edge set  $S$ , which consists of the edges of an image. We denote by  $n^s$  the vector valued measure representing the normal field on  $S$ , such that the representation  $D^s u = (u^+ - u^-)n^s$  holds for the singular part of the derivative. Here  $u^+$  and  $u^-$  are the upper and the lower (approximate lim sup and lim inf [23]) values at the edge  $S$ , respectively. This normal field is defined  $\mathcal{H}^{d-1}$  a.e. on  $S$ . Obviously,  $n^s$  is a morphological invariant as long as we consider continuous strictly monotone contrast modulating functions  $\beta$ .

Now, we focus on the regular part of the derivative. First, we adopt the classical gradient notion  $\nabla^{ac} u$  for the  $\mathcal{L}$  density of  $D^{ac}u$ , i. e.,  $D^{ac}u = \nabla^{ac} u \mathcal{L}$  [22]. As long as it is defined, the normalized gradient  $\frac{\nabla^{ac} u(x)}{\|\nabla^{ac} u(x)\|}$  is the outer normal on the upper topographic set  $l_{u(x)}^+[u]$  and thus again a morphological quantity. It is undefined on the flat image region  $F[u] := \{x \in \Omega : \nabla^{ac} u(x) = 0\}$ . We introduce  $n^{ac}$  as the normalized regular part of the gradient

$$n^{ac} = \chi_{\Omega \setminus F[u]} \frac{\nabla^{ac} u}{\|\nabla^{ac} u\|} \quad (3)$$

with support  $\Omega \setminus F$  and denote it the Gauss map of the image  $u$ .

With the regular normal  $n^{ac}$  and the singular normal measure  $n^s$  at hand, we are now able to redefine the morphology  $\mathcal{M}[u]$  of an image  $u$  as a unit length vector valued Radon measure on  $\Omega$  with

$$\mathcal{M}[u] = n^{ac} \mathcal{L} + n^s. \quad (4)$$

We call  $n^{ac} \mathcal{L}$  the regular morphology and  $n^s$  the singular morphology (cf. Fig. 2). It turns out that this new notion is equivalent to the above definition on sufficiently regular image functions. It completely describes the topographical shape information of the image  $u$ . If we skip the orientation of the vectors

$n^{ac}$  and  $n^s$  in (4) and replace them by the corresponding line subspaces we are able to treat general not only monotone contrast changes. This is actually reflected by our algorithm. In the next section, we aim to measure congruence of two image morphologies with respect to a matching deformation. In particular, we will make explicit use of the decomposition of image morphology derived here.

### III. THE VARIATIONAL APPROACH

Let us suppose that an initial template image  $u_T^0 \in L^2(\Omega)$  and an initial reference image  $u_R^0 \in L^2(\Omega)$  are given on an image domain  $\Omega \subset \mathbb{R}^d$ . Both images are assumed to be noisy. We aim for a simultaneous robust identification of smoothed and structural enhanced representations  $u_T, u_R \in SBV$  and a deformation  $\phi$ , which properly matches the underlying image morphologies (4), such that

$$\mathcal{M}[u_T \circ \phi] = \mathcal{M}[u_R].$$

Thus, we proceed as follows. The expected edge set in the reference image  $S_R := S_{u_R}$  is simultaneously treated as the pre image of the expected template edge set  $S_T := S_{u_T}$  under the deformation  $\phi$ , i. e.,

$$\phi(S_R) = S_T.$$

This will imply in the variational formulation that up to the orientation the singular morphologies have to be matched properly. The regular morphologies, which are also to be matched by the deformation, will be evaluated on the smoothed image representations  $u_T$  and  $u_R$  of both images. Thus, we consider as set of unknowns

$$u_T, u_R, S_T, \phi$$

and define three energy contributions, which together result in the actual variational formulation for a simultaneous edge segmentation, denoising and matching of images:

- a Mumford-Shah type energy  $E_{MS}[u_R, u_T, S_T, \phi]$  concerning about the actual edge segmentation and the proper correspondence of the singular morphologies,
- an energy  $E_{GM}[u_R, u_T, \phi]$  dealing with the alignment of the regular morphologies in terms of the Gauss maps of the smoothed image intensities  $u_R$  and  $u_T$  under the deformation  $\phi$ , and
- an energy  $E_{reg}[\phi]$  controlling the regularity of the deformation  $\phi$ .

With respect to the algorithmical realization we later consider a phase field approximation of the Mumford Shah energy  $E_{MS}$  picking up the approach by Ambrosio and Tortorelli [25]. The edge set  $S_T$  in the template image will be represented by a phase field function  $v$ , hence  $v \circ \phi$  can be regarded as the edge representation in the reference. In what follows let us consider the different energy contributions separately:

**Segmentation and matching of the singular morphology.** If we would minimize the Mumford-Shah functional (1) for  $u_T^0$  and  $u_R^0$  separately, we would obtain smooth representations  $u_T$

and  $u_R$  together with singularity sets  $S_T$  and  $S_R$ . Instead, we sum up these two functionals and replace the reference image edge set  $S_R$  by the pull back  $\phi^{-1}(S_T)$  of the template image edge set. Thus, a deformation  $\phi$  with  $S_R = \phi^{-1}(S_T)$  contributes to the minimization of the resulting combined energy. For any smooth deformation  $\phi$  the  $\mathcal{H}^{d-1}$  measure [23] of  $S_R$  can be controlled by the  $\mathcal{H}^{d-1}$  measure of  $S_T$  and the deformation  $\phi$ , i. e.,  $\mathcal{H}^{d-1}(S_R) = \int_{S_T} \det D\phi^{-1} \|D\phi D\phi^T n_T^s \cdot n_T^s\| d\mathcal{H}^{d-1}$  [39]. Indeed, the control of the deformation on such lower dimensional sets is analytically and numerically difficult. Hence, we omit the corresponding energy term here. Finally, the energy for the coupled Mumford-Shah segmentation in the reference and the template image is given by

$$\begin{aligned} E_{MS}[u_R, u_T, S_T, \phi] &= \frac{1}{2} \int_{\Omega} (u_R - u_T^0)^2 d\mathcal{L} \\ &+ \frac{\mu}{2} \int_{\Omega \setminus \phi^{-1}(S_T)} \|\nabla u_R\|^2 d\mathcal{L} + \eta \mathcal{H}^{d-1}(S_T) \\ &+ \frac{1}{2} \int_{\Omega} (u_T - u_T^0)^2 d\mathcal{L} + \frac{\mu}{2} \int_{\Omega \setminus S_T} \|\nabla u_T\|^2 d\mathcal{L} \end{aligned} \quad (5)$$

with  $\mu, \eta > 0$ . Let us remark that this energy does not care about the orientation of the normals on the singularity sets  $S_T$  and  $S_R$ . Thus, it is invariant not only under monotone contrast changes. So far, the deformation  $\phi$  is needed only on the singularity set  $S_T$  and thus it is highly under determined.

**Matching the regular image morphology.** The regular image morphology consists of the normal field  $n^{ac}$ . Hence, given arbitrary images  $u_T$  and  $u_R$  – later to be chosen as regularized representation of noisy initial images – we observe a perfect match of the regular morphology, if the deformation of the reference normal field  $n_R^{ac} := \frac{\nabla^{ac} u_R}{\|\nabla^{ac} u_R\|}$  (3) coincides with the template normals field  $n_T^{ac} := \frac{\nabla^{ac} u_T}{\|\nabla^{ac} u_T\|}$  at the deformed position. In fact, all level sets of the pull back template image  $u_T \circ \phi$  and the reference image  $u_R$  would then be nicely aligned (see Fig. 2). Let us denote by  $n_R^{ac, \phi}$  the transformation of the normal with respect to the deformation  $\phi$ . From the condition  $n_R^{ac, \phi} \cdot D\phi w = 0$  for tangent vectors  $w$  on level sets and the definition of the cofactor matrix  $\text{Cof } A := \det A A^{-T}$  [39] we deduce that

$$n_R^{ac, \phi} = \frac{\text{Cof } D\phi n_R^{ac}}{\|\text{Cof } D\phi n_R^{ac}\|} = \frac{\text{Cof } D\phi \nabla^{ac} u_R}{\|\text{Cof } D\phi \nabla^{ac} u_R\|}. \quad (6)$$

Now, we ask for a deformation  $\phi : \Omega \rightarrow \mathbb{R}^d$ , such that  $n_T^{ac} \circ \phi = n_R^{ac, \phi}$  (cf. Figure 2). Let us phrase this in terms of an energy integrand  $g : S^{d-1} \times S^{d-1} \rightarrow \mathbb{R}_0^+$ , which measures the misalignment of vectors on  $S^{d-1}$ . For instance, we might consider  $g(w, z) := \gamma \|(\mathbb{1} - w \otimes w)z\|^m$  for  $\gamma > 0$  and  $m \geq 2$ ,  $a \otimes b = ab^T$ . Let us emphasize that the resulting integrand is invariant with respect to the orientation of the normals and thus we are no longer restricted to monotone contrast changes in our notion of morphological equivalence. Thus, in a first attempt we consider the morphological registration energy

$$\int_{\Omega} g(n_T^{ac} \circ \phi, n_R^{ac, \phi}) d\mathcal{L},$$

where normals are evaluated on the initial images. Here, we face different problems, which have already been discussed in detail in [9]:

- Image normals  $n^{ac}$  are only defined apart from flat regions  $F$  and the above energy density turns out to be discontinuous at  $\partial F$ .
- Due to the renormalization of  $n_R^{ac,\phi}$  (6) by the factor  $\|\text{Cof } D\phi n_R^{ac}\|$ , the matching energy  $E_{GM}$  in general fails to be weakly lower semi-continuous on a suitable set of admissible deformations, a crucial condition to prove existence of minimizers in the so called direct method in the calculus of variations [39], [40].
- The evaluation of the regular morphology  $n^{ac}$  involves gradients. A direct computation of these gradients on noisy initial images  $u_T^0$  and  $u_R^0$  is surely questionable. Thus, an edge sensitive regularization is required to ensure robustness.

To avoid these shortcomings we modify the energy. At first, we use the regular image functions  $u_T$  and  $u_R$  from the above Mumford-Shah model for the computation of the regular image normal fields. Hence, the functional to be defined will depend on these unknowns as well. Furthermore, we take into account a new energy integrand  $g_0$ , which is a zero homogeneous extension of the integrand from our first trial, where we skip the above mentioned renormalization. We define

$$g_0(w, z, A) := \begin{cases} g\left(\frac{w}{\|w\|}, A \frac{z}{\|z\|}\right), & w \neq 0 \text{ and } z \neq 0, \\ 0, & \text{otherwise,} \end{cases} \quad (7)$$

for  $v, z \in \mathbb{R}^d$  and  $A \in \mathbb{R}^{d,d}$ . Based on this function we finally define the regular matching energy

$$E_{GM}[u_T, u_R, \phi] = \int_{\Omega} g_0(\nabla^{ac} u_T \circ \phi, \nabla^{ac} u_R, \text{Cof } D\phi) d\mathcal{L}. \quad (8)$$

Let us emphasize that this energy is still not continuous in  $\phi$ . The set of discontinuity is given by  $D_{GM} := D_R \cup \phi^{-1}(D_T) \cup \partial F_R \cup \partial(\phi^{-1}(F_T))$ , where  $D_R$  and  $D_T$  are the discontinuity sets of the regular image gradients  $\nabla^{ac} u_R$  are  $\nabla^{ac} u_T$ , respectively. Furthermore,  $F_R := F[u_R]$ ,  $F_T := F[u_T]$  are the flat regions in the reference and the template image, respectively. For the analytical treatment of these discontinuities we refer to [9].

**Controlling regularity of the deformation.** In a variational setting neither the matching energy for the singular morphology nor the one for the regular morphology uniquely identify the deformation  $\phi$ . Indeed, the problem is ill-posed. For instance, arbitrary reparametrizations of the level sets  $\partial l_c^+$  or the edge set  $S$ , and an exchange of level sets induced by the deformation do not change the energy. Thus, we have to regularize the variational problem. On the background of elasticity theory, we aim to model the image domain as an elastic body responding to forces induced by the matching energy. We have to emphasize, that we do not attempt to model the actual material of the objects represented by the image. Concerning the structure of the resulting functionals, the nonlinear elastic energy we are going to consider will be consistent with the nonlinearity in the regular matching energy. At first, let us briefly recall some background

from elasticity. For details we refer to the comprehensive introductions in the books by Ciarlet [41] and Marsden & Hughes [42]. We interpret  $\Omega$  as an isotropic elastic body and suppose that the regularization energy plays the role of an elastic energy while the matching energy can be regarded as an external potential. Furthermore we suppose  $\phi = \mathbb{1}$  to represent the stress free deformation. Let us consider the deformation of length, volume and for  $d = 3$  also area under a deformation  $\phi$ . It is well-known that the norm of the Jacobian of the deformation  $\|D\phi\|_2$  controls the isotropically averaged change of length under the deformation, where  $\|A\|_2 := \text{tr}(A^T A)^{\frac{1}{2}} = (\sum_{i,j} A_{ij} A_{ij})^{\frac{1}{2}}$  for  $A \in \mathbb{R}^{d,d}$ . Secondly, the local volume transformation under a deformation  $\phi$  is represented by  $\det D\phi$ . If  $\det D\phi$  changes sign local self-penetration may be observed. Furthermore for  $d = 3$ ,  $\|\text{Cof } D\phi\|_2$  is a proper measure for the averaged change of area. In general, we consider a so called polyconvex energy functional [39]

$$E_{reg}[\phi] := \int_{\Omega} W(D\phi, \text{Cof } D\phi, \det D\phi) d\mathcal{L}, \quad (9)$$

where  $W : \mathbb{R}^{d,d} \times \mathbb{R}^{d,d} \times \mathbb{R} \rightarrow \mathbb{R}$  is supposed to be convex. In particular, the built-in penalization of volume shrinkage, i. e.,  $W(A, C, D) \xrightarrow{D \rightarrow 0} \infty$ , enables us to successfully control singularity sets (cf. [9]). Such energies have already been introduced to the related optical flow problem by Hinterberger et al. [43]. But their focus was neither on morphological registration nor on the control of singularity sets. As an example, we can define a simple physically reasonable isotropic elastic energy for  $d = 3$ , which separately cares about length, area and volume deformation:

$$W(A, C, D) = \alpha_l \|A\|^p + \alpha_a \|C\|^q + \alpha_v [D^r + \beta D^{-s}] \quad (10)$$

with  $\alpha_l, \alpha_a, \alpha_v > 0, \beta$  implicitly defined by the property, that isometries minimize the energy, and  $r, s > 0$ . In nonlinear elasticity such material laws have been proposed by Ogden [44] and for  $p = q = 2$  we obtain the Mooney-Rivlin model [41]. We actually consider  $p = q = 2$  and  $r = s = 1$ .

**Collecting the different energy contributions.** Now, we have all the ingredients at hand to formulate the variational problem for a matching of the singular and regular image morphology combined with a simultaneous edge segmentation and denoising in the template and the reference image. We collect the matching energy (5) for the singular morphology, the matching energy (8) for the regular morphology, the elastic regularization energy (9) and define the global energy

$$E[u_R, u_T, S_T, \phi] := E_{MS}[u_R, u_T, S_T, \phi] + E_{GM}[u_R, u_T, \phi] + E_{reg}[\phi]. \quad (11)$$

Even for very simple image pairs  $u_R^0$  and  $u_T^0$  we expect the resulting energy landscape to be very complicated. To address this issue, we will not restrict to a single fine scale problem but consider an embedding into a scale of problems to be solved from coarse to fine. This scale will be induced by a phase field approximation of the energy  $E_{MS}$ . The scale parameter will

correspond to the width of the phase transition region. In particular, we will make use of the multiple scales in the numerical algorithm. Together with a corresponding hierarchy of function space this will enable us to derive an effective and efficient algorithm.

#### IV. MULTIPLE SCALES INDUCED BY A PHASE-FIELD APPROXIMATION

The singularity set  $S_T$  as an explicit argument is difficult to treat algorithmically. For the approximation of the edge set  $S_T$  in [45] a level set formulation has been proposed. This approach is in particular well-suited as long as the edge set is closed and topologically simple. Whereas this may be convenient in some cases, for example, when the initialization allows a certain degree of user control to preselect certain features, it may also be ambiguous and tedious in other cases. Here, we propose a phase-field formulation (2) in the spirit of Ambrosio and Tortorelli [25] to gain more flexibility and in addition to incorporate a simple multi scale into the model. Concerning the coupling of the edge segmentation in the reference and the template image we proceed analogously to the Mumford Shah model above. Let us introduce an auxiliary variable  $v$ , describing the singularity set  $S_T$  of the image  $u_T$ . At the same time  $v \circ \phi$  is taken into account to describe the edge set  $S_R$  in the image  $u_R$ . Apart from  $S_T$  and  $S_R = \phi^{-1}(S_T)$  we aim for  $v \approx 1$ . The phase field should vanish on  $S_T$  and  $\phi^{-1}(S_T)$ , respectively. As in the original segmentation approach [25] a scale parameter  $\epsilon$  controls the thickness of the region with small phase field values. These requirements are reflected by the energy

$$\begin{aligned} E_{AT}^\epsilon[u_R, u_T, v, \phi] := & \\ & \frac{1}{2} \int_{\Omega} \left( (u_R - u_R^0)^2 + (u_T - u_T^0)^2 \right) d\mathcal{L} \\ & + \frac{\mu}{2} \int_{\Omega} \left( (v^2 \circ \phi + k_\epsilon) \|\nabla u_R\|^2 + (v^2 + k_\epsilon) \|\nabla u_T\|^2 \right) d\mathcal{L} \\ & + \int_{\Omega} \left( \eta \epsilon \|\nabla v\|^2 + \frac{\eta}{4\epsilon} (v - 1)^2 \right) d\mathcal{L}, \quad (12) \end{aligned}$$

where  $k_\epsilon = o(\epsilon)$ . The first integral measures the deviation of  $u_R$  and  $u_T$  to the data in  $L^2$  and can be regarded as a fidelity term as in the Mumford Shah approach. The second integral forces the signature  $v^2$  to be small where  $u_T$  has steep gradients and, correspondingly,  $v^2 \circ \phi$  to be small where  $\nabla u_R$  is large. Furthermore, for fixed signature and fixed deformation, the smoothness of the images  $u_R$  and  $u_T$  is controlled apart from the edge sets, i. e., steep gradients of  $u_T$  are penalized where  $v \not\approx 0$  and analogously for  $u_R$ . Finally, the third integral approximates the  $\mathcal{H}^{d-1}$  measure of the edge set and forces  $v \approx 1$  apart from edges. Not aligning edges in  $u_R$  with edges in  $u_T \circ \phi$  would result in a  $v$  which reflects both edge sets separately (cf. Fig. 9 and Fig. 15).

In that case we would count them twice with respect to the length measurement. Hence, it is preferable to align them as long as the cost for the elastic deformation measured in terms of  $E_{reg}$  is relatively low.

As already mentioned, the total energy  $E[\cdot]$  is highly non-linear and the energy landscape will be very complicated. Thus, minimizing already on the highest resolution with the fully developed deformation is not feasible. In particular the energies



Fig. 3

CONTRAST INVARIANT MATCHING: WE HAVE INVERTED, MOVED AND DISTORTED THE PEPPERS IMAGE (LEFT) TO OBTAIN A TEMPLATE IMAGE (MIDDLE). ON THE RIGHT THE INITIAL MISFIT IS SHOWN.

controlling the registration of regular and singular morphology cause many local minima in the energy landscape. We take a multiscale approach, solving a sequence of matching problems ranging from coarse to fine scales. This type of method is frequently applied and well understood in image processing [46]. It remains for us to define a scale of energies. Thus, we consider the parameter  $\epsilon$  in the phase field approximation  $E_{AT}^\epsilon$  as scale parameter. The width of the edge regions indicated by small values of  $v$  is expected to be proportional to  $\epsilon$ . For decreasing  $\epsilon$  we will obtain successively sharper regularized images  $u_T$  and  $u_R$ . This implicitly introduces a scale in the energy  $E_{GM}$  as well. In explicit the gradients  $\nabla u_T$  and  $\nabla u_R$  corresponding to  $u_T$  and  $u_R$  are expected to be smoother for larger  $\epsilon$ . Thus, we no longer have to distinguish regular and singular gradients. To focus only on the regular morphology in this energy contribution - in particular not measuring edges - we mask out a gradient comparison in the vicinity of edges. Therefore, the integrand is multiplied by  $v^2 \circ \phi$  and we obtain

$$E_{GM}^\epsilon[u_T, u_R, v, \phi] = \int_{\Omega} v^2 \circ \phi g_0(\nabla u_T \circ \phi, \nabla u_R, \text{Cof } D\phi) d\mathcal{L}. \quad (13)$$

Finally, gathering the energy contributions from (12), (13) and (9) we define a scale of global approximate energies

$$\begin{aligned} E^\epsilon[u_R, u_T, v, \phi] := & E_{AT}^\epsilon[u_R, u_T, v, \phi] \\ & + E_{GM}^\epsilon[u_R, u_T, v, \phi] + E_{reg}[\phi]. \quad (14) \end{aligned}$$

depending on the scale parameter  $\epsilon$ . We refer to Fig. 3 and 4 for results achieved via a relaxation of this energy. Furthermore, Fig. 5 shows the decay of the  $L^2$  difference of the computed deformation and the prescribed deformation - which we have chosen in the construction of this test case - depending on the iteration counter of our numerical algorithm. We expect the computed solution to minimize the elastic energy over all deformations which match the two image morphologies. But our prescribed deformation is not chosen as this optimal elastic deformation. Thus, it will not coincide with the prescribed one and a residual difference in the deformation remains.

Now, we consider a sequence of regularization parameters  $(\epsilon_k)_{k=1, \dots, K}$ . On the coarsest scale, we start with  $\epsilon_K$  of the order 1 and consider successively refined  $\epsilon_k = \frac{1}{2}\epsilon_{k+1}$ . In the numerical algorithm, the parameter  $\epsilon_1$  is supposed to be of the order of the pixel or voxel size. In essence, the energy land-

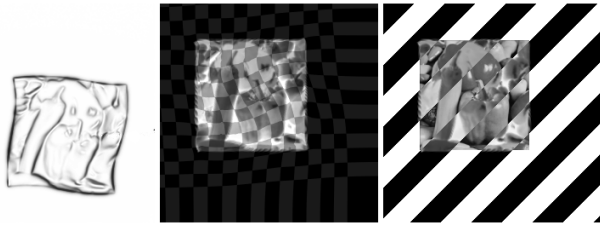


Fig. 4

REGISTRATION RESULT FOR INPUT DATA FROM FIG. 3: THE FINAL PHASE FIELD FUNCTION  $v$  IS DEPICTED ON THE LEFT. THE IMAGE IN THE MIDDLE SHOWS A PLOT OF THE DEFORMATION DUE TO A RELAXATION OF THE COMBINED ENERGY  $E_{AT}^\epsilon + E_{reg} + E_{GM}^\epsilon$ , I. E., THE REGISTRATION OF DISCONTINUITY SETS AND LEVEL SETS. ON THE RIGHT ALTERNATING SLICES OF THE REFERENCE AND THE PULLED BACK TEMPLATE IMAGE ALLOW A VISUAL VALIDATION OF THE MATCHING RESULT.

scape is smoothed, enabling “basin catching” at coarse levels to provide good starting guesses for subsequently finer levels.

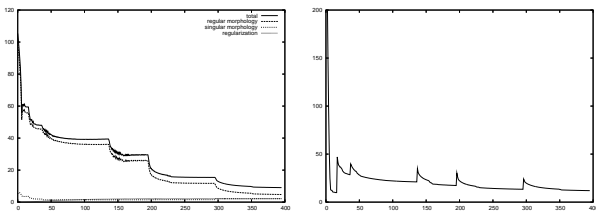


Fig. 5

LEFT: ENERGY DECAY PLOT THE TOTAL ENERGY, REGULAR MORPHOLOGICAL ENERGY, SINGULAR MORPHOLOGICAL ENERGY AND THE REGULARIZATION ENERGY. ALL ENERGIES ARE EVALUATED ON THE FINEST GRID LEVEL AFTER PROLONGATING THE CURRENTLY COMPUTED DEFORMATION IN EACH STEP. RIGHT: TOTAL ENERGY EVALUATED ON THE CURRENT LEVEL USED FOR ADAPTIVE STEP-SIZE CONTROL.

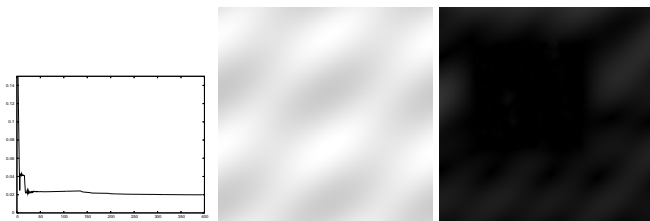


Fig. 6

LEFT: PLOT OF THE DECAY OF THE  $L^2$  DIFFERENCE BETWEEN THE COMPUTED DEFORMATION AND THE KNOWN EXACT DEFORMATION FOR THE SEQUENCE OF DEFORMATIONS COMPUTED IN THE MINIMIZATION ALGORITHM ON MULTIPLE SCALES. THE MIDDLE AND RIGHT IMAGES SHOW THE ERROR DENSITY OF THE DEFORMATION BEFORE AND AFTER THE MINIMIZATION, SCALED BETWEEN 0 (BLACK) AND 0.26 (WHITE).

Note, that it is not necessary to compute the exact minimizer on coarse scales. Instead we apply a descent method (cf. Section V) and stop iterating as soon as the update is sufficiently small. In practice this proves to be a good heuristic to ensure

that at the time we stop on level  $k$  with a deformation  $\phi^k$ , this deformation is already in the contraction region of the global minimum on the next finer scale  $k + 1$ . Furthermore, in the finite element algorithm we will resolve coarse scales on coarse grids (cf. Section V). Consequently most iterations of the algorithm are spent on coarse grids with corresponding performance benefits.

## V. ENERGY RELAXATION AND NUMERICAL IMPLEMENTATION

The energy introduced above depends on four unknown functions, the scalar valued regularized images  $u_T, u_R$ , the scalar phase field  $v$  and the vector valued deformation  $\phi$ . In what follows, we will outline an energy relaxation method in the continuous setting. Secondly, we will briefly describe how to discretize this approach based on finite elements. Furthermore, for the convenience of the reader, a comprehensive collection of variations of the different energy contributions with respect to the different unknown is given in the appendix.

Apart from  $E_{GM}$  the energy depends quadratically on  $u_T, u_R$  and  $v$ . Thus, the corresponding necessary conditions to be fulfilled by a minimizer, i. e., the Euler Lagrange equations with respect to these variables, turn into linear problems. Indeed, in contrast to the original approach of [47], where approximating elliptic but non-quadratic functionals have been used, our approximation of the Mumford Shah type energy for the matching of the singular morphology follows (2) and gives rise for this simplification. We refer for instance to [48], [49] and for the numerical treatment to [50].

In the relaxation scheme for the deformation, which actually describes the image matching, we treat  $u_T, u_R$ , and  $v$  in a quasi stationary way. In fact, the iterative relaxation proceeds as follows:

For given images and deformation, we optimize w.r.t. the phase field  $v$ . In a next step, we then optimize for the regularized images  $u_T$  and  $u_R$  for given  $\phi$  and already optimized  $v$ . Finally, we consider one gradient descent step for the global energy w.r.t. the deformation. This procedure is repeated until convergence.

The variation  $\delta_\phi E^\epsilon$  of the global energy in  $\phi$  is a functional acting on infinitesimal deformations. We apply a regularizing operator  $\mathcal{A}$  to map this energy variation onto a regularized direction in the space of deformation. In abstract terms this regularized direction is the gradient direction with respect to a regularized metric  $(\cdot, \cdot)_\mathcal{A}$  on the space of deformation, where  $\mathcal{A}$  is essentially the inverse of the corresponding metric tensor. This approach differs from the “natural gradient” approach by Trouné [28], where the definition of a metric on infinitesimal deformations along geodesics in shape space (cf. also Miller, Trouné and Younes [1]) has a strong direct impact on the resulting matching. In our context, which is more related to the early approach of Christensen, Miller and Rabbitt, the metric on variations of the matching functional is applied to stabilize the numerical relaxation via a gradient descent and does not influence the minimizer of the functional itself. For details we refer to [51]. In the actual implementation we consider a multigrid approximation of  $\mathcal{A} = (\mathbb{1} - \frac{\sigma^2}{2}\Delta)^{-1}$ , with  $\mathbb{1}$  being the identity

matrix, similar to the one proposed in [52]. We treat this as an approximation of a Gaussian filter, or in terms of a regularizing metric we choose  $(\psi, \zeta)_{\mathcal{A}} = \int_{\Omega} \psi \cdot \zeta + \frac{\sigma^2}{2} D\psi : D\zeta \, d\mathcal{L}$ , where “ $\cdot$ ” indicates the Euclidean scalar product in  $\mathbb{R}^d$  and “ $:$ ” is a scalar product on matrices with  $A : C = \text{tr}(A^T B)$  for  $A, B \in \mathbb{R}^{d,d}$ . As step size control in the descent step we consider Armijo’s rule [53]. For the sake of simplicity of the exposition we might assume Dirichlet boundary conditions  $\phi(x) = x$  on the image domain boundary  $\partial\Omega$ . We refer to [54] and [36] for an attenuation towards an only partial correspondence of the images. Next, let us sketch the method in pseudo code notation:

```

Energy-Relaxation( $u_T^0, u_R^0$ ) {
  initialize ( $u_T^{K,0}, u_R^{K,0}, \phi^{K,0}$ )  $\leftarrow$  ( $u_T^0, u_R^0, \mathbb{1}$ );
  for  $k = K, \dots, 1$  do {
     $l = 0$ ;
    do {
       $v^{k,l+1} = \arg \min E^{\epsilon_k}[u_T^{k,l}, u_R^{k,l}, v, \phi^{k,l}]$ ;
      ( $u_T^{k,l+1}, u_R^{k,l+1}$ ) =  $\arg \min_{u_T, u_R} E^{\epsilon_k}[u_T, u_R, v^{k,l+1}, \phi^{k,l}]$ ;
      For given smoothing operator  $\mathcal{A}$  update
       $\phi^{k,l+1} = \phi^{k,l} - \tau^l \mathcal{A} \delta_{\phi} E^{\epsilon_k}[u_T^{k,l+1}, u_R^{k,l+1}, v^{k,l+1}, \phi^{k,l}]$ ;
      for a suitable time step  $\tau^l$ ;
       $l \leftarrow l + 1$ ;
    } until ( $\|\phi^{k,l} - \phi^{k,l-1}\| \leq \delta_k$ );
    set ( $u_T^{k-1,0}, u_R^{k-1,0}, \phi^{k-1,0}$ )  $\leftarrow$  ( $u_T^{k,l}, u_R^{k,l}, \phi^{k,l}$ );
  }
}

```

Here,  $k$  is the current scale,  $l$  the number of already executed relaxation steps on this scale, and  $\|\cdot\|$  the usual  $L^2$  norm on the space of deformations. All functions are indexed by the scale  $k$  and the relaxation step  $l$ . On the coarse scale we initialize the deformation  $\phi^{K,0}$  with the identity deformation  $\mathbb{1}(x) = x$ . We stop the inner iteration on each scale, if the norm of the deformation update  $\phi^{k,l} - \phi^{k,l-1}$  is below a threshold  $\delta_k = C\epsilon_k$ .

To break down the different steps, we have to consider the variations of the different energy contributions. The computation of these derivatives is a straightforward, albeit involved, application of the chain rule. For the readers convenience we provide this calculations in full detail in the appendix below.

**Governing partial differential equations.** From  $\delta_v E^{\epsilon_k} = 0$ , we deduce that for given images  $u_T, u_R$  and deformation  $\phi$  the updated phase field  $v$  solves the linear, elliptic partial differential equation

$$0 = -2\eta\epsilon\Delta v + \frac{\eta}{2\epsilon}(v-1) + \mu\|\nabla u_T\|^2 v + \frac{\mu\|\nabla u_{R\circ\phi^{-1}}\|^2 + 2g_0(\nabla u_T, \nabla u_{R\circ\phi^{-1}}, \text{Cof } D\phi\circ\phi^{-1})}{\det D\phi\circ\phi^{-1}}$$

with homogeneous Neumann boundary condition  $\nabla v \cdot n = 0$ , where  $n$  is the outer normal on the image domain boundary  $\partial\Omega$ .

Furthermore, for fixed  $v$  and  $\phi$  the reconstructed images  $u_R$  and  $u_T$  are solutions of the following non linear PDEs derived

from the necessary conditions  $0 = \delta_{u_R} E^{\epsilon_k} = \delta_{u_T} E^{\epsilon_k}$ .

$$\begin{aligned} 0 &= u_R - u_R^0 - \mu \operatorname{div} \left( (v^2 \circ \phi + k_{\epsilon}) \nabla u_R \right) \\ &\quad - \operatorname{div} \left( v^2 \circ \phi \partial_z g_0(\nabla u_T \circ \phi, \nabla u_R, \text{Cof } D\phi) \right), \\ 0 &= u_T - u_T^0 - \mu \operatorname{div} \left( (v^2 + k_{\epsilon}) \nabla u_T \right) \\ &\quad - \operatorname{div} \left( \frac{v^2 \partial_w g_0(\nabla u_T, \nabla u_{R\circ\phi^{-1}}, \text{Cof } D\phi\circ\phi^{-1})}{\det D\phi\circ\phi^{-1}} \right), \end{aligned}$$

where  $\partial_z$  and  $\partial_w$  denote the variations of  $g_0$  w.r.t. its first and second arguments. Again, we assume natural boundary conditions  $\nabla u_T \cdot n = \nabla u_R \cdot n = 0$  on the image domain boundary. For details on the derivation of these differential equations we refer to Chapter 5.5 in [54]. In the current implementation we neglect the impact of the ongoing segmentation process on the variation of the energy concerned with the regular morphology and consider the following simplification in the method:

$$(u_T^{k,l+1}, u_R^{k,l+1}) = \arg \min_{u_T, u_R} E_{AT}^{\epsilon}[u_T, u_R, v^{k,l+1}, \phi^{k,l}]$$

Thus, the last term on the right hand side is skipped in both equations above and  $u_T$  and  $u_R$  turn out to be solution of the linear PDEs:

$$\begin{aligned} 0 &= u_R - u_R^0 - \mu \operatorname{div} \left( (v^2 \circ \phi + k_{\epsilon}) \nabla u_R \right) \\ 0 &= u_T - u_T^0 - \mu \operatorname{div} \left( (v^2 + k_{\epsilon}) \nabla u_T \right). \end{aligned}$$

Even though, we no longer actually minimize the global energy, the proposed restricted energy relaxation already leads to satisfying edge segmentation and matching results.

**Spatial discretization by finite elements.** Now, we describe the actual spatial discretization by finite elements and the construction of a discrete multi scale. We consider images as piecewise multilinear (bilinear in our 2D applications) finite element functions on a regular image domain. Each pixel or voxel value corresponds to a node of the regular mesh. For the ease of implementation we suppose dyadic resolutions of the images with  $2^L + 1$  pixels or voxels in each direction. Thus, we are able to build a hierarchy on grids with  $2^l + 1$  nodes in each direction for  $l = L, \dots, 0$ . We restrict every finite element function via a trivial restriction operation to any of these coarse grid spaces. We apply these finite element space not only for the representation of discrete images but also for the discretization of the phase field  $v$  and the  $d$  components of the deformation  $\phi$ . The construction of the multigrid hierarchy allows to solve coarse scale problems in our multi scale approach on coarse grids. Indeed, scale  $k$  is resolved on the corresponding  $l(k)$ th grid level (e.g. with  $l(k) = k$ ). From the above still continuous relaxation scheme, we derive a fully practical numerical algorithm in a straightforward way. Following the general finite element procedure, the discretization of the PDEs for the phase field  $v$  and the regularized images  $u_T, u_R$  leads to linear systems of equations, which are solved via a preconditioned conjugate gradient method [55]. In the assembly of these linear systems we apply on each grid cell a third order Gaussian quadrature rule.

For the variation of the energy with respect to  $\phi$ , we consider the same quadrature rule and assemble a vector of variations

in all basis directions on the space of discrete deformations. Next, this vector is smoothed applying one multigrid  $V$  cycle corresponding to a standard finite element implementation of the differential operator  $\mathbb{1} - \frac{\sigma^2}{2} \Delta$ . For details we refer to [51], [9].

At various places, we have to evaluate discrete functions  $U$  at pushed forward or pulled back positions under a discrete deformation  $\Phi$ . In both cases we replace the exact evaluation of these functions by a simple and effective interpolation. Indeed, we replace  $U \circ \Phi$  by  $\mathcal{I}(U \circ \Phi)$ , where  $\mathcal{I}$  is the classical Lagrangian interpolation on the grid nodes. Thus, each grid node is mapped under the deformation  $\Phi$  onto the image domain,  $U$  is evaluated at these positions and these values define our new finite element function. Analogously,  $U \circ \Phi^{-1}$  is replaced by  $\mathcal{I}(U \circ (\mathcal{I} \circ \Phi)^{-1})$ . Here, we proceed as follows. We map each grid cell under the deformation onto the image domain. Next we identify all grid nodes, which are located on this deformed cell. These grid nodes are then mapped back under the inverse local deformation. Now, interpolation is applied to retrieve requested values of the finite element function  $U$ . Inversion of multilinear deformation leads to nonlinear equations. To avoid this shortcoming, we cut each cell virtually into simplices. On these simplices affine functions approximate in a straightforward way the multilinear functions. Thus, we replace the regular cells in the retrieval algorithm by the simplices and end up with piecewise affine inverse mappings.

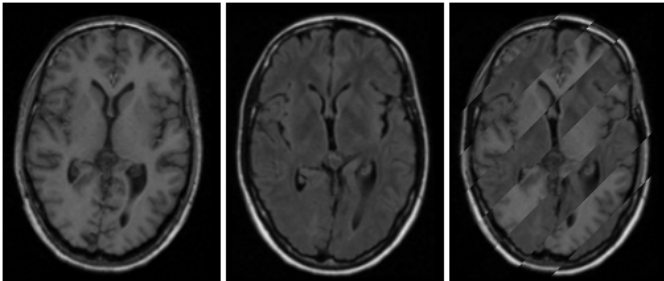


Fig. 7

THE REGISTRATION OF FLAIR AND T1-WEIGHTED MAGNETIC RESONANCE BRAIN IMAGES IS CONSIDERED. THE INITIAL DATA, A REFERENCE T1 IMAGE (LEFT) AND A TEMPLATE FLAIR IMAGE (MIDDLE) AND THE INITIAL MISMATCH (RIGHT) ARE SHOWN. THE MISFIT IS ILLUSTRATED BY OVERLAYING THE REFERENCE WITH STRIPES OF THE TEMPLATE.

## VI. RESULTS

We have applied the relaxation algorithm to several different scenarios in order to underline the importance of coupling the different energy contributions. As our first example, shown in Fig 1, we have considered a square on a white background as the reference image. As the template we consider this square shifted to the bottom right but with an additional non-rigid but smooth deformation in the interior. The object has strong edges on the outline, that correspond to the singular morphology, while in the interior the morphology is completely regular

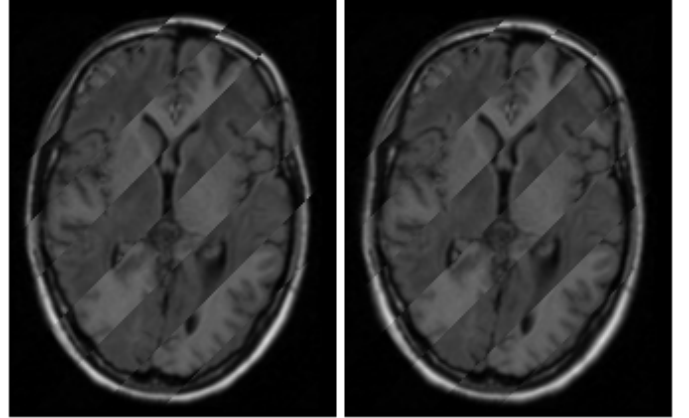


Fig. 8

FOR THE INITIAL DATA SHOWN IN FIG. 7, THE LEFT IMAGE SHOWS THE RESULTING REGISTRATION RESULT ONLY TAKING INTO ACCOUNT THE REGULARIZATION AND THE REGULAR MORPHOLOGY ENERGY  $E_{GM}^\epsilon + E_{reg}$ . IN PARTICULAR REGIONS WITH SMOOTHLY VARYING INTENSITY ARE ALREADY IN GOOD CORRESPONDENCE, BUT STRONG EDGES IN THE INTERIOR AND CLOSE TO THE SKULL ARE NOT MATCHED PROPERLY. THE RESULTS CAN BE SIGNIFICANTLY IMPROVED BY A RELAXATION OF THE TOTAL ENERGY  $E_{GM}^\epsilon + E_{AT}^\epsilon + E_{reg}$  SHOWN ON THE RIGHT. WE OBSERVE A GOOD REGISTRATION ALREADY IN THE FIRST CASE. MEASURED IN IMAGE PIXELS, SEVERAL, ANATOMICALLY DISTINCT DISCONTINUITIES ARE VERY CLOSE TO EACH OTHER AT THE SKULL OUTLINE, WHICH CAUSES THE PARTICULAR DIFFICULTY IN THIS EXAMPLE AND ALSO LEADS TO THE REMAINING ARTIFACT ON THE TOP OF THE IMAGE.

and characterized by the geometry of the level sets. After relaxation of the Mumford Shah type energy in combination with the hyperelastic regularization energy, it is possible to recover the simple translation, while the interior remains completely rigid. After adding the energy term  $E_{GM}^\epsilon$ , which cares about a proper matching of the regular morphology, it is also possible to recover the interior deformation. In these computations we have set  $\mu = \eta = 0.1$ ,  $\gamma = 0$  resp. 100,  $\mu = \eta = 0.1$ ,  $\alpha_l = 10$ ,  $\alpha_v = 40$ ,  $\sigma_k = 3h_k$  and  $\epsilon_k = \frac{1}{20}h_k$ . Another example in the same spirit is shown in Fig. 3 and 4, where a reference and a template image that differs by a large distortion and a contrast change are registered properly.

As a first real world example we have considered the matching of two magnetic resonance images of the human brain: the reference in a standard T1-weighting and the template as a FLAIR weighted MR image. To render the test problem even more difficult, we have in addition artificially deformed the FLAIR image by a rotational twist in the interior of the skull. Figures 7 shows the the initial images and the initial mismatch on the right. Figure 8 compares the registration results with and without the energy  $E_{AT}^\epsilon$ . The combined method clearly outperforms the registration solely based on a matching of the regular morphology. The regular morphology however takes care of alignment of low-contrast shape information such as in the region of the ventricle, which is characterized by level set geometry rather than strong contrast. Figure 9 shows a comparison

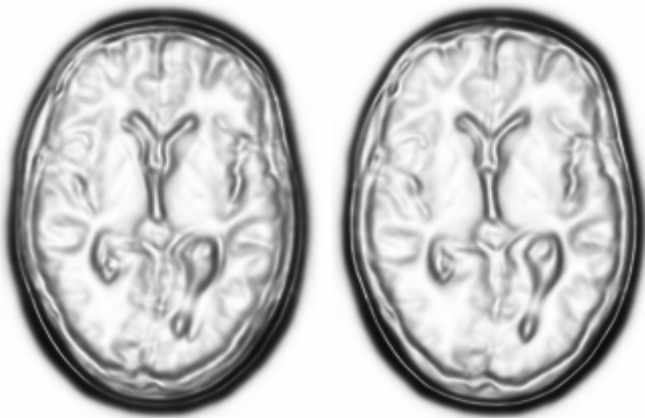


Fig. 9

THE PHASE FIELD  $v$  CORRESPONDING TO THE REGISTRATION IN FIGURE 7. LEFT: INITIAL PHASE FIELD. RIGHT: PHASE FIELD AFTER ALIGNMENT.

of the initial phase field function evaluated on the finest resolution after the first iteration of the relaxation algorithm with the final phase field. The initial mismatch can be observed in  $v$  by the fact that edges from both images are visible separately, while in the final result  $v$  represents coinciding edges of  $u_T$  and  $u_R \circ \phi^{-1}$ . Hence, in the latter case the overall length of the joint discontinuity set is shorter. These computations were performed with parameters  $\mu = \eta = 0.1$ ,  $\gamma = 0$  resp. 100,  $\alpha_l = 200$ ,  $\alpha_v = 40$ ,  $\sigma_k = 5h_k$  and  $\epsilon_k = \frac{1}{20}h_k$ .

We have applied our method also to 3D medical image registration problems and present here first results, where we concentrate on a matching only of the singular morphology. In particular in 3D a cascadic multiscale approach turned out to be indispensable to ensure an efficient numerical implementation. Fig. 10 depicts an application where brain structures of MR scans of two different patients with varying image contrast are to be matched. The underlying 3D images consist of  $257^3$  voxels and thus  $3 \cdot 257^3$  unknowns in the nodal vector of deformation. Our results demonstrate that without any pre-registration the algorithm is able to generate a fairly good match. Nevertheless, due to the structural differences in the two brains the capabilities of the algorithm are locally limited basically by the built in regularity control of the elastic deformation. Furthermore, Fig. 11 actually deals with multimodal matching. It shows the matching of a pair of 3D MR T1-weighted and positron density images. The underlying image resolution is  $129 \times 257 \times 257$ . This application in particular shows the limitation of our approach based on a mathematical notion of morphology in case of significantly different medical image morphologies. The algorithm applied to raw data without any preprocessing is still capable to generate a reasonable overall matching for instance of the cortex outline or of the skull. But it significantly suffers from the local deviation of medical morphology which requires prior knowledge on non local anatomy from the underlying mathematical morphology with its purely local definition. In both 3D applications we have chosen a slightly different sets of model parameters:  $\mu = 16$ ,  $\eta = 1.6$ ,  $\gamma = 0$ ,  $\alpha_l = 1$ ,  $\alpha_v = 1$ ,

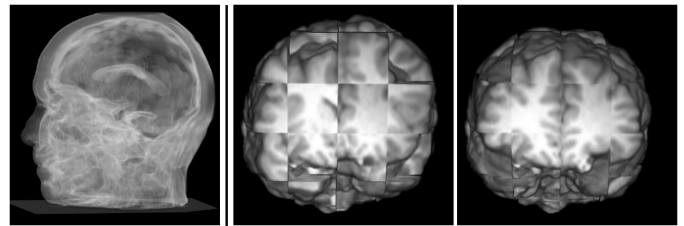


Fig. 10

ON THE LEFT THE 3D PHASEFIELD CORRESPONDING TO AN MR IMAGE IS SHOWN. FURTHERMORE, THE MATCHING OF TWO MR BRAIN IMAGES OF DIFFERENT PATIENTS IS DEPICTED. WE USE A VOLUME RENDERER BASED ON RAY CASTING (VTK) FOR A 3D CHECKERBOARD WITH ALTERNATING BOXES OF THE REFERENCE AND THE PULL BACK OF THE TEMPLATE IMAGE TO SHOW THE INITIAL MISMATCH OF MR BRAIN IMAGES OF TWO DIFFERENT PATIENTS (MIDDLE) AND THE RESULTS OF OUR MATCHING ALGORITHM (RIGHT).

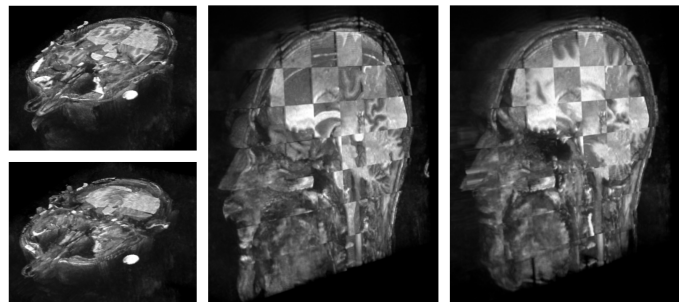


Fig. 11

A PAIR OF 3D T1-WEIGHTED MR AND POSITRON DENSITY IMAGES IS REGISTERED. THE TWO IMAGES ARE RENDERED AGAIN USING RAY CASTING OF A SLICED 3D CHECKERBOARD WITH ALTERNATING BOXES CORRESPONDING TO THE DIFFERENT IMAGES. THE INITIAL MISMATCH (UPPER LEFT AND MIDDLE) IS COMPARED WITH THE FINAL MATCHING RESULT (LOWER LEFT AND RIGHT) ON AN AXIAL SLICE AND A SAGITTAL SLICE.

compared to the 2D case. The numerical parameter  $\sigma_k$  and  $\epsilon_k$  are the same.

This application in particular underlines that edge segmentation not only helps image matching but vice versa matching can help edge segmentation. To emphasize this, we compute a matching of a pair of 2D slides of the pair of T1-weighted MR and positron density images. In Fig. 12 we compare the phase field in the first iteration of our algorithm with its clearly visible mismatch of the two morphologies and the final joint phase field function. The latter indicates that weaker edges in particular in the positron density image are strengthened via a pull back of edges from the MR image onto to the positron density image.

Finally, we demonstrate the applicability of the method by registering two different facial texture maps. Figure 13 shows again the reference and template images in the top row, while in the bottom row we compare registration based on the full model and a restricted energy  $E_{AT}^{\epsilon_k} + E_{reg}^{\epsilon_k}$  neglecting the regu-

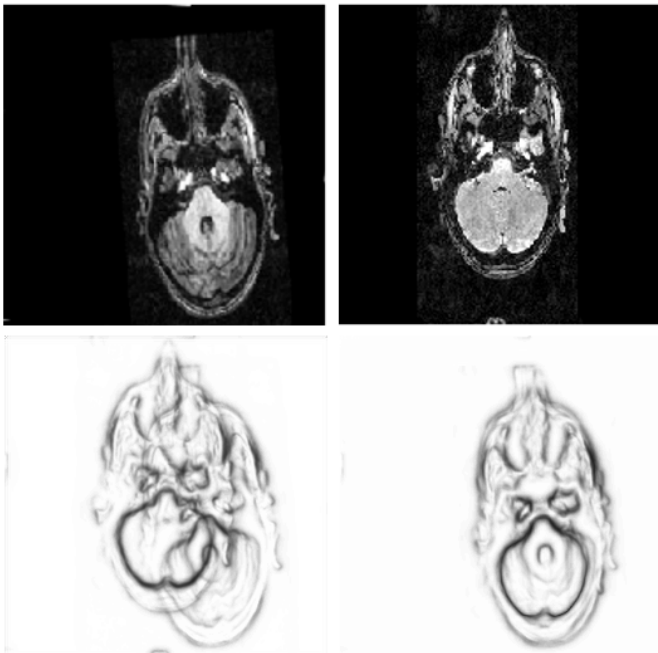


Fig. 12

A PAIR OF 2D SLICES THROUGH THE 3D POSITRON DENSITY (TOP LEFT) AND THE T1-WEIGHTED MR IMAGE (TOP RIGHT LEFT) IS REGISTERED.

THE PHASE FIELD COMPUTED IN THE FIRST ITERATION OF OUR ALGORITHM (BOTTOM LEFT) SHOWS THE INITIAL MISMATCH AND IN PARTICULAR FOR THE POSITRON DENSITY IMAGE LOCALLY WEAK EDGE SEGMENTATION. ON THE BOTTOM RIGHT THE JOINT PHASEFIELD OF THE TWO IMAGES AFTER THE REGISTRATION IS DEPICTED. HERE, WEAK POSITRON DENSITY EDGES ARE MATCHED ONTO STRONG MR EDGES.

lar morphology. In the restricted case, we observe an acceptable match of the outline at sharp edges in the region of the mouth, the eyebrows and the eyes. However, the full method ensures a much better registration capturing further geometric information. The deformation plots in the top row underline this improvement. Figure 14 pinpoints the differences of the different matching approaches. As in the previous example, Figure 15 illustrates the energetic improvement due to the interplay of the deformation and the phase-field function, reducing the length of the overall interface by alignment of edges. In these computations the chosen parameters are  $\mu = \eta = 0.1, \gamma = 0$  resp. 10,  $\alpha_l = 10, \alpha_v = 5, \sigma_k = 5h_k$  and  $\epsilon_k = \frac{1}{20}h_k$ .

## VII. CONCLUSIONS

We have introduced a generalized notion of image morphology which distinguishes regular contour sets encoded by the regular field of image normals from edge sets represented by a concentrated measure valued normal field. Based on this concept a variational approach for multi modal image registration has been introduced and various applications in 2D and 3D demonstrate the capabilities of this new method. Its major characteristic is that we jointly segment edges via a Mumford–Shah approach and register image morphologies. This direct combination of two imaging tasks ensures not only that prior



Fig. 13

A FACIAL TEXTURE MATCHING PROBLEM. INITIAL REFERENCE TEXTURE MAP  $u_R$  (LEFT), INITIAL TEMPLATE  $u_T$  (MIDDLE) AND THE INITIAL MISFIT PLOT ON THE (RIGHT).

knowledge on edges improved the registration results but at the same time registration can improve locally weak edge segmentation via a correspondence to stronger edges in the other image. The variational approach comes along with phase field approximations for the Mumford–Shah functional simultaneously for both images, where the edge set of one image is implicitly represented by the pull back of the edge set from the other image under the deformation. Picking up concepts from rational mechanics a third, polyconvex, elastic energy cares about the registration of the regular normal fields and finally regularity of the deformation is ensured by a fourth, nonlinear, again polyconvex elastic energy, which is also known to guarantee a one-to-one deformation [57]. The phase field approximation introduces a multiscale parameter, which is coupled with the image resolution in a cascading finite element algorithm. Interesting research perspectives are

- a detailed comparison of our variational method based on a local energy density with the non local, long range interaction encoded in the joint histogram analysis of mutual information statistics and a combination of both algorithms,
- a definition of metrics in shape space which reflects our refined notion of morphology and would allow us to compute geodesic paths and not only matching deformations, and
- a detailed comparison of medical and mathematical morphology, which might help to better apply concepts developed here to complex, multimodal registration problems in medical imaging which go beyond the principle study of applicability investigated here.

## ACKNOWLEDGMENT

We would like to thank Frithjof Kruggel from the MPI Neurosciences in Leipzig for kindly providing the PD and T1 test case. Furthermore, we thank Carlo Schaller from the Department of Neurosurgery, Bonn for discussions on medical morphology as well as Benjamin Berkels for support with the volume renderer.

## REFERENCES

- [1] M. Miller, A. Trounev, and L. Younes, “On the metrics and Euler-Lagrange equations of computational anatomy,” *Annual Review of Biomedical Engineering*, vol. 4, pp. 375–405, 2002, in print.
- [2] U. Grenander and M. I. Miller, “Computational anatomy: An emerging discipline,” *Quarterly Appl. Math.*, vol. LVI, no. 4, pp. 617–694, 1998.

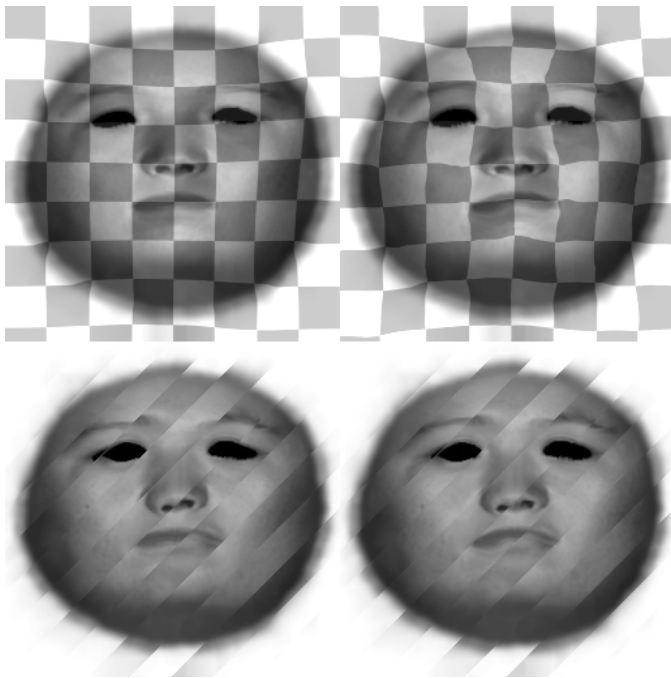


Fig. 14

RESULTS FOR THE FACIAL TEXTURE MATCHING PROBLEM GIVEN IN 13.

THE TOP ROW SHOWS THE DEFORMED TEMPLATE THAT HAS BEEN OVERLAID BY A UNIFORM CHECKERBOARD PATTERN. ON THE LEFT THE REGULAR MORPHOLOGY HAS NOT BEEN TAKEN INTO ACCOUNT, HENCE, MAINLY THE FACE OUTLINE AND STRONG EDGES ARE MATCHED PROPERLY. CONSIDERING THE ENTIRE ENERGY FUNCTIONAL SIGNIFICANTLY IMPROVES THE RESULT (RIGHT). THE DEFORMATION IS CHARACTERIZED BY A MUCH HIGHER VARIABILITY. THE BOTTOM ROW DISPLAYS WITH ALTERNATING STRIPES THE CORRESPONDING REFERENCE AND PULLED BACK TEMPLATE IMAGES TO ENABLE A VALIDATION OF THE MATCHING RESULTS.



Fig. 15

THE PHASE FIELD  $v$  CORRESPONDING TO THE MATCHING RESULTS IN FIGURE 13. LEFT: INITIAL PHASE FIELD. RIGHT: PHASE FIELD AFTER ALIGNMENT.

- [3] J. Modersitzki and B. Fischer, "Fast diffusion registration," *Special Issue of Contemporary Mathematics*, AMS, 2000.
- [4] J. P. Thirion, "Image matching as a diffusion process: An analogy with maxwell's demon," *Medical Imag. Analysis*, vol. 2, pp. 243–260, 1998.
- [5] P. A. Viola and W. Wells III, "Alignment by maximization of mutual information," Tech. Rep. AITR-1548, 1995.
- [6] W. Wells, P. Viola, H. Atsumi, S. Nakajima, and R. Kikinis, "Multi-modal volume registration by maximization of mutual information," 1996.
- [7] A. e. a. Collignon, "Automated multi-modality image registration based on information theory," in *Proc. Conf. Information Processing in Medical Imaging*, Y. Bizais, Ed. Kluwer Academic Publishers, 1995, pp. pp. 263–274.
- [8] M. Mellor and M. Brady, "Phase mutual information as a similarity measure for registration," *Medical Image Analysis*, vol. Volume 9 (4), pp. 330–343, 2005.
- [9] M. Droske and M. Rumpf, "A variational approach to non-rigid morphological registration," *SIAM Appl. Math.*, vol. 64, no. 2, pp. 668–687, 2004.
- [10] Y. N. Young and D. Levy, "Registration-based morphing of active contours for segmentation of CT-scans," *Mathematical Biosciences and Engineering*, vol. 2, no. 1, pp. 79–96, 2005.
- [11] J.-P. Thirion and A. Gourdon, "Computing the differential characteristics of iso-intensity surfaces," *Computer Vision and Image Understanding*, vol. 61 (2), pp. 190–202, 1995.
- [12] T. Kapur, L. Yezzi, and L. Zöllei, "A variational framework for joint segmentation and registration," *IEEE CVPR - MMBIA*, 2001.
- [13] T. F. Chan and L. A. Vese, "Active contours without edges," *IEEE Transactions on Image Processing*, vol. 10, no. 2, pp. 266 – 277, 2001.
- [14] G. Unal and G. Slabaugh, "Coupled PDEs for non-rigid registration and segmentation," in *IEEE Computer Society International Conference on Computer Vision and Pattern Recognition (CVPR)*, 2005.
- [15] Y. Chen, S. Thiruvankadam, F. Huang, K. S. Gopinath, and R. W. Brigg, "Simultaneous segmentation and registration for functional mr images," *ICPR*, vol. 01, pp. 10 747–, 2002.
- [16] P. P. Wyatt and J. A. Noble, "MAP MRF joint segmentation and registration," in *MICCAI (1)*, 2002, pp. 580–587.
- [17] O. F'eron and A. Mohammad-Djafari, "Image fusion and unsupervised joint segmentation using a HMM and MCMC algorithms," *J. of Electronic Imaging*, 2004, to appear.
- [18] T. Dohi and R. Kikinis, Eds., *Medical Image Computing and Computer-Assisted Intervention - MICCAI 2002, 5th International Conference, Tokyo, Japan, September 25-28, 2002, Proceedings, Part I*, ser. Lecture Notes in Computer Science, vol. 2488. Springer, 2002.
- [19] G. Matheron, *Random Sets and Integral Geometry*. John Wiley N.Y., 1975.
- [20] V. Caselles, B. Coll, and J. M. Morel, "Topographics maps and local contrast invariance in natural images," *Int. J. Comp. Vision*, vol. 33, pp. 5–27, 1999.
- [21] D. Mumford and J. Shah, "Optimal approximation by piecewise smooth functions and associated variational problems," *Comm. Pure Appl. Math.*, vol. 42, pp. 577–685, 1989.
- [22] L. Ambrosio, N. Fusco, and D. Pallara, *Functions of bounded variation and free discontinuity problems*. Oxford University Press, 2000.
- [23] L. C. Evans and R. F. Gariepy, *Measure Theory and Fine Properties of Functions*. CRC Press, 1992.
- [24] L. Rudin, S. Osher, and E. Fatemi, "Nonlinear total variation based noise-removal," *Physica D*, vol. 60, pp. 259–268, 1992.
- [25] L. Ambrosio and V. M. Tortorelli, "On the approximation of free discontinuity problems," *Boll. Un. Mat. Ital. B*, vol. 6, no. 7, pp. 105–123, 1992.
- [26] L. G. Brown, "A survey of image registration techniques," *ACM Computing Surveys*, vol. 24, no. 4, pp. 325–376, 1992.
- [27] P. A. van den Elsen, E.-J. J. Pol, and M. A. Viergever, "Medical image matching: A review with classification," *IEEE Engineering in Medicine and Biology*, vol. 12, pp. 26–39, 1993.
- [28] A. Trounev, "Diffeomorphisms groups and pattern matching in image analysis," *International Journal of Computer Vision*, vol. 28 (3), pp. 213–221, 1998.
- [29] M. F. Beg, M. Miller, A. Trounev, and L. Younes, "Computing large deformation metric mappings via geodesic flows of diffeomorphisms," *International Journal of Computer Vision*, vol. 61, no. 2, pp. 139–157, February 2005.
- [30] R. Bajcsy and C. Broit, "Matching of deformed images," in *Int. Conf. Pattern Recognition*, 1982, pp. 351–353.
- [31] G. E. Christensen, S. C. Joshi, and M. I. Miller, "Volumetric transformations of brain anatomy," *IEEE Trans. Medical Imaging*, vol. 16, no. 6, pp. 864–877, 1997.
- [32] G. E. Christensen, R. D. Rabbitt, and M. I. Miller, "Deformable templates using large deformation kinematics," *IEEE Trans. Medical Imaging*, vol. 5, no. 10, pp. 1435–1447, 1996.
- [33] C. A. Davatzikos, R. N. Bryan, and J. L. Prince, "Image registration based on boundary mapping," *IEEE Trans. Medical Imaging*, vol. 15, no. 1, pp. 112–115, 1996.

- [34] J. Modersitzki and B. Fischer, "Curvature based image registration," *JMIV*, vol. 18, no. 1, 2003.
- [35] I. Cohen, "Nonlinear variational method for optical flow computation," in *Proceedings of the 8th Scandinavian Conference on Image Analysis*. Tromsø, Norway: IAPR, June 1993, pp. 523–530.
- [36] N. Litke, M. Droske, M. Rumpf, and P. Schröder, "An image processing approach to surface matching," in *Proc. Symposium on Geometry Processing*, 2005.
- [37] L. Alvarez, F. Guichard, P. L. Lions, and J. M. Morel, "Axioms and fundamental equations of image processing," *Arch. Ration. Mech. Anal.*, vol. 123, no. 3, pp. 199–257, 1993.
- [38] G. Sapiro, *Geometric Partial Differential Equations and Image Analysis*. Cambridge University Press, 2001.
- [39] B. Dacorogna, *Direct Methods in the Calculus of Variations*, ser. Appl. Math. Sciences 78. Springer-Verlag, Berlin, 1989.
- [40] L. Evans, *Partial Differential Equations*, reprint with corrections ed. Providence Rhode Island: American Mathematical Society, 2002.
- [41] P. G. Ciarlet, *Three-Dimensional Elasticity*. Elsevier, New York, 1988.
- [42] J. E. Marsden and T. J. R. Hughes, *Mathematical foundations of Elasticity*. Prentice-Hall, Englewood Cliffs, 1983.
- [43] W. Hinterberger, O. Scherzer, C. Schnörr, and J. Weickert, "Analysis of optical flow models in the framework of calculus of variations," Numerical Functional Analysis and Optimization, Revised version of Technical Report No. 8/2001, Computer Science Series, University of Mannheim, Germany., Tech. Rep., 2001.
- [44] R. W. Ogden, *Non-Linear Elastic Deformations*. John Wiley, 1984.
- [45] M. Droske and W. Ring, "A Mumford-Shah level-set approach for geometric image registration," *SIAM Appl. Math.*, 2005, to appear.
- [46] L. Alvarez, J. Weickert, and J. S'anchez, "A scale-space approach to nonlocal optical flow calculations," in *Scale-Space Theories in Computer Vision. Second International Conference, Scale-Space '99, Corfu, Greece, September 1999*, ser. Lecture Notes in Computer Science; 1682, M. Nielsen, P. Johansen, O. F. Olsen, and J. Weickert, Eds. Springer, 1999, pp. 235–246.
- [47] L. Ambrosio and V. M. Tortorelli, "Approximation of functionals depending on jumps by elliptic functionals via  $\Gamma$ -convergence," *Comm. Pure Appl. Math.*, vol. 43, pp. 999–1036, 1990.
- [48] G. Belletini and A. Coscia, "Discrete approximation of a free discontinuity problem," *Num. Funct. Anal. Optim.*, vol. 15, pp. 201–224, 1994.
- [49] T. J. Richardson and S. K. Mitter, "A variational formulation based edge focussing algorithm," *Sadhana Acad. P. Eng. S.*, vol. 22, no. 4, pp. 553–574, 1997.
- [50] B. Bourdin, "Image segmentation with a Finite Element method," *ESIAM: Mathematical Modelling and Numerical Analysis*, vol. 33, no. 2, pp. 229–244, 1999.
- [51] U. Clarenz, M. Droske, and M. Rumpf, "Towards fast non-rigid registration," in *Inverse Problems, Image Analysis and Medical Imaging, AMS Special Session Interaction of Inverse Problems and Image Analysis*, vol. 313. AMS, 2002, pp. 67–84.
- [52] S. Henn and K. Witsch, "Iterative multigrid regularization techniques for image matching," *SIAM J. Sci. Comput.*, vol. 23 No 4, pp. 1077–1093, 2001.
- [53] P. Kosmol, *Optimierung und Approximation*. de Gruyter Lehrbuch, 1991.
- [54] M. Droske, "On variational problems and gradient flows in image processing," Ph.D. dissertation, Universität Duisburg-Essen, 2005.
- [55] W. Hackbusch, *Iterative Solution of Large Sparse Systems of Equations*, ser. Applied Mathematical Sciences, F. John, J. E. Marsden, and L. Sirovich, Eds. Springer, 1994, vol. 95.
- [56] "The visualization toolkit," <http://www.vtk.org>.
- [57] J. Ball, "Discontinuous equilibrium solutions and cavitation in nonlinear elasticity," *Phil. Trans. R. Soc. Lond.*, vol. 306, pp. 557–611, 1982.
- [58] —, "Global invertibility of Sobolev functions and the interpenetration of matter," *Proc. Roy. Soc. Edinburgh*, vol. 88A, pp. 315–328, 1988.

## APPENDIX: ENERGY VARIATIONS

Here, we give explicit formulas for the variation of the different energy contributions in directions of the unknown functions  $u_R, u_T, v, \phi$  required in the algorithm above. We denote by  $\langle \delta_w E, \psi \rangle$  a variation of an energy  $E$  with respect to a parameter function  $w$  in a direction  $\psi$ . The variation of  $E_{AT}^\epsilon$  (12) with respect to  $v$  in direction  $\zeta$  is given

by

$$\begin{aligned} \langle \delta_v E_{AT}^\epsilon, \zeta \rangle &= \mu \int_{\Omega} \|\nabla u_T\|^2 v \zeta \, d\mathcal{L} + \frac{\|\nabla u_R \circ \phi^{-1}\|^2}{\det D\phi \circ \phi^{-1}} v \zeta \, d\mathcal{L} \\ &\quad + \eta \int_{\Omega} 2\epsilon \nabla v \cdot \nabla \zeta + \frac{1}{2\epsilon} (v-1) \zeta \, d\mathcal{L}. \end{aligned} \quad (15)$$

Here, on account of the hyperelastic regularization  $E_{reg}$  we assume that  $\phi$  is invertible [58] and have applied an integral transform. Furthermore, for  $E_{GM}^\epsilon$  (13) one achieves

$$\begin{aligned} \langle \delta_v E_{GM}^\epsilon, \zeta \rangle &= \int_{\Omega} 2(v \circ \phi) (\zeta \circ \phi) g_0(\nabla u_T \circ \phi, \nabla u_R, \text{Cof } D\phi) \, d\mathcal{L} \\ &= \int_{\Omega} 2v \zeta \frac{g_0(\nabla u_T, \nabla u_R \circ \phi^{-1}, \text{Cof } D\phi \circ \phi^{-1})}{\det D\phi \circ \phi^{-1}} \, d\mathcal{L}. \end{aligned}$$

Next, we consider variations of the energies (12) and (13) with respect to  $u_T$  and  $u_R$  and get

$$\begin{aligned} \langle \delta_{u_R} E_{AT}^\epsilon, \vartheta \rangle &= \int_{\Omega} (u_R - u_R^0) \vartheta + \mu(v^2 \circ \phi + k_\epsilon) \nabla u_R \cdot \nabla \vartheta \, d\mathcal{L}, \\ \langle \delta_{u_T} E_{AT}^\epsilon, \vartheta \rangle &= \int_{\Omega} (u_T - u_T^0) \vartheta + \mu(v^2 + k_\epsilon) \nabla u_T \cdot \nabla \vartheta \, d\mathcal{L}, \\ \langle \delta_{u_T} E_{GM}^\epsilon, \vartheta \rangle &= \int_{\Omega} v^2 \circ \phi \, \partial_w g_0(\nabla u_T \circ \phi, \nabla u_R, \text{Cof } D\phi) (\nabla \vartheta \circ \phi) \, d\mathcal{L}, \\ &= \int_{\Omega} v^2 \frac{\partial_w g_0(\nabla u_T, \nabla u_R \circ \phi^{-1}, \text{Cof } D\phi \circ \phi^{-1}) (\nabla \vartheta)}{\det D\phi \circ \phi^{-1}} \, d\mathcal{L}, \\ \langle \delta_{u_R} E_{GM}^\epsilon, \vartheta \rangle &= \int_{\Omega} v^2 \circ \phi \, \partial_z g_0(\nabla u_T \circ \phi, \nabla u_R, \text{Cof } D\phi) (\nabla \vartheta) \, d\mathcal{L}. \end{aligned}$$

For the derivatives of the zero-homogeneous integrand  $g_0$  (7) in directions  $y$  occurring above, we evaluate

$$\begin{aligned} \partial_w g_0(w, z, A)(y) &= \partial_w g(w, Az)(P[w] \|w\|^{-1} y), \\ \partial_z g_0(w, z, A)(y) &= \partial_z g(w, Az)(x)(AP[z] \|z\|^{-1} y). \end{aligned}$$

Here, we have taken into account that  $D_w \frac{w}{\|w\|} = \frac{1}{\|w\|} P[w]$  where  $P[w]$  is the projection matrix  $(\mathbb{1} - \frac{w}{\|w\|} \otimes \frac{w}{\|w\|})$ . In case of the integrand  $g(w, z) = \gamma \|P[w]z\|^2$  we observe

$$\begin{aligned} \partial_z g(w, z)(y) &= 2\gamma P[w]z \cdot y \\ \partial_w g(w, z)(y) &= -2\gamma \left( \frac{P[w]y}{\|w\|} \otimes \frac{w}{\|w\|} + \frac{w}{\|w\|} \otimes \frac{P[w]y}{\|w\|} \right) z \cdot z \end{aligned}$$

Finally, for the gradient descent step with respect to the deformation, we have to evaluate the variation of the energy (14) in  $\phi$  and compute

$$\begin{aligned} \langle \delta_\phi E_{AT}^\epsilon, \psi \rangle &= \mu \int_{\Omega} \|\nabla u_R\|^2 v \circ \phi (\nabla v \circ \phi) \cdot \psi \, d\mathcal{L}, \\ \langle \delta_\phi E_{GM}^\epsilon, \psi \rangle &= \int_{\Omega} 2(v \circ \phi) (\nabla v \circ \phi) \cdot \psi g_0(M) \, d\mathcal{L} \\ &\quad + \int_{\Omega} (v^2 \circ \phi) \partial_A g_0(M) (\partial_A \text{Cof } (D\phi)(D\psi)) \, d\mathcal{L} \\ &\quad + \int_{\Omega} (v^2 \circ \phi) \partial_w g_0(M) (D^2 u_T \circ \phi) \cdot \psi \, d\mathcal{L}, \\ \langle \delta_\phi E_{reg}, \psi \rangle &= \int_{\Omega} \partial_A W(Q) : D\psi + \partial_C W(Q) : \partial_A \text{Cof } (D\phi)(D\psi) \, d\mathcal{L} \\ &\quad + \int_{\Omega} \partial_D W(Q) \partial_A \det(D\phi)(D\psi) \, d\mathcal{L}, \end{aligned}$$

where we have used the abbreviations  $M = (\nabla u_T \circ \phi, \nabla u_R, \text{Cof } D\phi)$  and  $Q = (D\phi, \text{Cof } D\phi, \det D\phi)$ . Consistent to the above proposed

simplification we again neglect the impact of the edge segmentation on the regular morphology extraction and hence skip the last term on the right hand side of the equation for  $\delta_\phi E_{GM}^\epsilon$  in the concrete implementation. Furthermore, we apply the following formulas for derivatives

$$\begin{aligned}\partial_A g_0(w, z, A)(C) &= \partial_z g\left(\frac{w}{\|w\|}, A \frac{z}{\|z\|}\right) \left(C \frac{z}{\|z\|}\right), \\ \partial_A \text{Cof}(A)(C) &= \det A (\text{tr}(A^{-1}C)A^{-T} - A^{-T}C^T A^{-T}), \\ \partial_A \det(A)(C) &= \det A \text{tr}(A^{-1}C)\end{aligned}$$

In case of the concrete example (10) for the regularization energy (9) we calculate

$$\begin{aligned}\partial_A W(A, C, D) &= p \alpha_l \|A\|^{p-2} A, \\ \partial_C W(A, C, D) &= q \alpha_a \|C\|^{q-2} C, \\ \partial_D W(A, C, D) &= \alpha_v (rD^{r-1} - \beta_s D^{-(s+1)}).\end{aligned}$$